NAVAL POSTGRADUATE SCHOOL

MONTEREY, CALIFORNIA

THESIS

ENVIRONMENTAL FACTORS THAT PROMOTE TROPICAL CYCLONE TORNADO OUTBREAKS

by

Christopher R. Mortenson

December 2021

Thesis Advisor:	John M. Peters
Second Reader:	Joel W. Feldmeier, Office of Naval Research Global

THIS PAGE INTENTIONALLY LEFT BLANK

REPORT DOCUMENTATION PAGE			*Form Approved OMB No. 0704-0188*

1. AGENCY USE ONLY *(Leave blank)*	**2. REPORT DATE** December 2021	**3. REPORT TYPE AND DATES COVERED** Master's thesis

4. TITLE AND SUBTITLE ENVIRONMENTAL FACTORS THAT PROMOTE TROPICAL CYCLONE TORNADO OUTBREAKS	**5. FUNDING NUMBERS**
6. AUTHOR(S) Christopher R. Mortenson	
7. PERFORMING ORGANIZATION NAME(S) AND ADDRESS(ES) Naval Postgraduate School Monterey, CA 93943-5000	**8. PERFORMING ORGANIZATION REPORT NUMBER**
9. SPONSORING / MONITORING AGENCY NAME(S) AND ADDRESS(ES) N/A	**10. SPONSORING / MONITORING AGENCY REPORT NUMBER**

11. SUPPLEMENTARY NOTES The views expressed in this thesis are those of the author and do not reflect the official policy or position of the Department of Defense or the U.S. Government.

12a. DISTRIBUTION / AVAILABILITY STATEMENT Approved for public release. Distribution is unlimited.	**12b. DISTRIBUTION CODE** A

13. ABSTRACT (maximum 200 words)

Difficulty in predicting tropical cyclone (TC) tornado outbreaks persists as a problematic issue in meteorology. Research has shown some TCs produce many tornadoes when they make landfall while others do not, independent of intensity. Additionally, we don't know how shear and entrainment might be different between high-end and low-end TC tornado outbreak events. Therefore, an in-depth examination of individual storm parameters at the time of outbreak will provide new insight into distinguishing the dynamics of prolific and non-prolific tornadic outbreak TCs. TC tornado outbreaks from 1979–2020 are analyzed using the NOAA climate reanalysis dataset (NCEP-DOE Reanalysis 2) to investigate the synoptic environment of 23 high-end prolific and 23 low-end non-prolific tornadic TC systems. Furthermore, research focuses on comparing the environmental factors of surface to 6 km and surface to 1 km bulk wind difference (BWD), 1–6 km average relative humidity (RH), MLCAPE, MLECAPE, and MLECAPE P20 for prolific TC tornado events to non-prolific events. We were able to produce two soundings for initial conditions from composite plots to run a non-hydrostatic Cloud Model 1 (CM1). Two runs of a composite of prolific and non-prolific TC tornado events are used to test the differences in vertical velocity, surface and 1 km vorticity. The results will help better understand TC tornado outbreak environmental factors for improved forecast predictions and resource protection.

14. SUBJECT TERMS tropical cyclones, TC, NOAA, tornadoes	**15. NUMBER OF PAGES** 53
	16. PRICE CODE

17. SECURITY CLASSIFICATION OF REPORT	**18. SECURITY CLASSIFICATION OF THIS PAGE**	**19. SECURITY CLASSIFICATION OF ABSTRACT**	**20. LIMITATION OF ABSTRACT**
Unclassified	Unclassified	Unclassified	UU

NSN 7540-01-280-5500

Standard Form 298 (Rev. 2-89)
Prescribed by ANSI Std. 239-18

THIS PAGE INTENTIONALLY LEFT BLANK

Approved for public release. Distribution is unlimited.

ENVIRONMENTAL FACTORS THAT PROMOTE TROPICAL CYCLONE TORNADO OUTBREAKS

Christopher R. Mortenson
Lieutenant, United States Navy
BS, North Carolina State University, 2013

Submitted in partial fulfillment of the
requirements for the degree of

MASTER OF SCIENCE IN METEOROLOGY AND PHYSICAL OCEANOGRAPHY

from the

NAVAL POSTGRADUATE SCHOOL
December 2021

Approved by: John M. Peters
Advisor

Joel W. Feldmeier
Second Reader

Wendell A. Nuss
Chair, Department of Meteorology

THIS PAGE INTENTIONALLY LEFT BLANK

ABSTRACT

Difficulty in predicting tropical cyclone (TC) tornado outbreaks persists as a problematic issue in meteorology. Research has shown some TCs produce many tornadoes when they make landfall while others do not, independent of intensity. Additionally, we don't know how shear and entrainment might be different between high-end and low-end TC tornado outbreak events. Therefore, an in-depth examination of individual storm parameters at the time of outbreak will provide new insight into distinguishing the dynamics of prolific and non-prolific tornadic outbreak TCs. TC tornado outbreaks from 1979–2020 are analyzed using the NOAA climate reanalysis dataset (NCEP-DOE Reanalysis 2) to investigate the synoptic environment of 23 high-end prolific and 23 low-end non-prolific tornadic TC systems. Furthermore, research focuses on comparing the environmental factors of surface to 6 km and surface to 1 km bulk wind difference (BWD), 1–6 km average relative humidity (RH), MLCAPE, MLECAPE, and MLECAPE P20 for prolific TC tornado events to non-prolific events. We were able to produce two soundings for initial conditions from composite plots to run a non-hydrostatic Cloud Model 1 (CM1). Two runs of a composite of prolific and non-prolific TC tornado events are used to test the differences in vertical velocity, surface and 1 km vorticity. The results will help better understand TC tornado outbreak environmental factors for improved forecast predictions and resource protection.

THIS PAGE INTENTIONALLY LEFT BLANK

TABLE OF CONTENTS

I. INTRODUCTION....1

II. DATA AND METHODS....5
- **A. METHODS FOR REANALYSIS....5**
- **B. MODEL SETUP....10**
- **C. METHODS FOR ANALYSIS....11**

III. RESULTS....13
- **A. STORM FOLLOWING COMPOSITES....13**
- **B. COMPOSITE SOUNDING PROFILES....22**
- **C. MODEL SIMULATIONS....25**

IV. SUMMARY AND CONCLUSIONS....27

LIST OF REFERENCES....31

INITIAL DISTRIBUTION LIST....35

THIS PAGE INTENTIONALLY LEFT BLANK

LIST OF FIGURES

Figure 1. TC Tornado Outbreak 1979–2020 Dataset 5

Figure 2. TC Center Location at Time of Tornado Outbreak 8

Figure 3. Storm Following Surface to 6 km Bulk Wind Difference Composites 14

Figure 4. Comparison Composite Surface to 6 km Bulk Wind Difference 14

Figure 5. Storm Following Surface to 1 km Bulk Wind Difference Composites 15

Figure 6. Comparison Composite Surface to 1 km Bulk Wind Difference 16

Figure 7. Storm Following 1–6 km Average Relative Humidity Composites 17

Figure 8. Comparison Composite 1–6 km Average Relative Humidity 18

Figure 9. Storm Following MLCAPE, MLECAPE, MLECAPE P20 Composites 20

Figure 10. Comparison Composite MLCAPE, MLECAPE, MLECAPE P20 21

Figure 11. High-End Composite Environmental Sounding 23

Figure 12. High-End Composite Environmental Wind Profile 23

Figure 13. Low-End Composite Environmental Sounding 24

Figure 14. Low-End Composite Environmental Wind Profile 24

Figure 15. Vertical Velocity and Vorticity Time Series 26

THIS PAGE INTENTIONALLY LEFT BLANK

LIST OF TABLES

Table 1. Tropical Cyclone Basic Information for High-End Events 7

Table 2. Tropical Cyclone Basic Information for Low-End Events 7

Table 3. CM1 Model Configuration 10

THIS PAGE INTENTIONALLY LEFT BLANK

LIST OF ACRONYMS AND ABBREVIATIONS

BWD	bulk wind difference
CAPE	convective available potential energy
CM1	Cloud Model 1
DOE	Department of Energy
ECAPE	entrainment convection available potential energy
EIL	effective inflow layer
LBC	lateral boundary conditions
MLCAPE	mean layer convective available potential energy
MLECAPE	mean layer entrainment convective available potential energy
NCAR	National Center for Atmospheric Research
NCEP	National Center for Environmental Prediction
NHC	National Hurricane Center
PSL	Physical Science Laboratory
RH	relative humidity
SR	storm relative
SRH	storm relative helicity
TC	tropical cyclone
w	vertical velocity

THIS PAGE INTENTIONALLY LEFT BLANK

ACKNOWLEDGMENTS

To my wife, Dana, and daughter, Avery, I could not ask for a more supportive, loving family in my life. To my advisor, Dr. John Peters; LCDR Mike Adamski; and the METOC staff: your guidance and mentorship allowed this research project to be possible and my time at NPS to be rewarding. Thank you.

THIS PAGE INTENTIONALLY LEFT BLANK

I. INTRODUCTION

Tropical cyclone (TC) tornadoes have long been known to occur within the outer bands and inner envelope of a landfalling or remnant TC that transitioned to an extratropical system. Often occurring in the form of tornado outbreaks, TC tornadoes range from several tornadoes to several dozen (Baker et al. 2009). Many have occurred along the Gulf Coast and in the Southeast of the United States (Schultz and Cecil 2009). Previous studies have shown that many of the tornadoes either occur along with convective outer bands of TCs or well in advance of the tropical storm or hurricane-force winds. Hence, their forecasting becomes a crucial complex problem (Gentry 1983). Edwards (2012) observed that damaging winds from TC tornadoes mainly occur away from the area of hurricane-force winds, in regions where hurricane preparations may not have been performed. Furthermore, TCs that do not become upgraded to hurricane status of winds greater than 65kts can still produce destructive tornadic outbreaks accounting for extensive damage. While many landfalling TCs can produce tornadoes, not all TCs become prolific tornado outbreak events, which adds to the forecast challenge of ensuring the public is adequately prepared.

TC tornado outbreaks present societal impacts with the ability to produce significant damage. In 2005 TC tornado damage proved to be very costly when estimates totaled over $100 million (Schultz and Cecil 2009). Gentry (1983) states that tornadoes from Hurricane Allen resulted in over $70 million in damage in coastal regions of the state of Texas. Gentry (1983) also observed that one of the most destructive TC tornadoes in Texas history caused extensive damage to the Austin Airport and nearby residential areas resulting in $50 million in damage. Although many TC tornadoes are less intense than the classic Midwest Great Plains tornadoes, their severity cannot be overlooked. Grazulis (1990) shows how there are exceptions to less intense TC tornados, where he states, that Hurricane Carla was the first to spawn a violent F4 TC tornado. This one TC tornado from Hurricane Carla caused around 25% fatalities in Texas as it made landfall at Galveston, TX, on 12 September 1961. Which began as a waterspout that then moved on land, this tornado killed a total of 8 people injuring 55 more.

The types of storms that most commonly produce tornadoes are called supercells. Supercells feature a persistent updraft with substantial vertical velocity *w* (Edwards 2012). Additionally, Weisman and Klemp's (1982,1984) research showed that for supercell thunderstorms to develop its important for substantial vertical wind shear to be present in the atmosphere. Vertical wind shear is essentially the change in wind speed and/or direction with height from the surface moving aloft in the atmosphere. Commonly assessed from the surface to 5 km or 6 km and referred to as bulk wind difference (BWD) to obtain the magnitude of a layer shear vector. Research shows that the wind shear over these depths, referred to hereafter as "deep-layer shear," is a skillful discriminator of supercells from other convective modes (Thompson et al. 2003; Houston et al. 2008). Furthermore, strong deep-layer shear often occurs in conjunction with strong low-level storm-relative (SR) flow, allowing for updrafts to become wider and deep layer shear to be a good discriminator of storm mode (Peters et al. 2019, 2020b). Whereas low-level shear is generally obtained from the surface to 1 km or 3 km, a lower threshold for low-level shear is necessary for supercells. However, low-level shear is not a good discriminator of supercells from nonsupercells. Instead, low-level storm-relative flow is more useful in determining the difference between supercell and nonsupercell tornadoes (Rasmussen and Blanchard 1998; Thompson et al. 2003; Peters et al. 2020b). As wind shear increases, interaction between a supercells updraft, and downdraft can strongly influence and increase convective storm organization; conversely, weaker wind shear generally results in convection that is weaker and less organized overall. Furthermore, supercells in high shear environments result in higher upward accelerations and enhanced updraft speed opposed to those in less sheared environments (Peters et al. 2019). These different shear layers can vary independently of each other; therefore, both layers will be the focus of this research

Convective available potential energy (CAPE) is another important environmental parameter for forecasting the development of deep convection (Moncrieff and Miller 1976). Mean layer convective available potential energy (MLCAPE) is more commonly used today over standard surface-based CAPE and is calculated from the lowest 100 mb above ground level using a parcel that consists of mean layer values of moisture and temperature (NOAA 2021). However, there are well-known flaws that limit the utility of

MLCAPE including how it neglects mixing/entrainment; therefore, this study will also examine mean layer entraining convective available potential energy (MLECAPE) for the role of entrainment about the effective inflow layer (EIL), which modulates updraft buoyancy and *w* (Peters et al. 2020a). MLECAPE was used since it might be a better metric for how buoyant the updrafts are as opposed to regular MLCAPE. For instance, its often discussed that TC tornadoes occur with lower MLCAPE than traditional Midwest tornados. However, due to high relative humidity (RH), MLECAPE is more similar between TC and non-TC tornado environments. Additionally, Sueki and Niino (2016) showed that including entrainment of environmental air into the calculation of CAPE results in greater skill in spatially identifying the tornadic regions of tropical cyclones.

Operational forecasting and warning for TC tornadoes is difficult and involves shorter lead times than non-TC tornadoes. For instance, tornado vortex signatures are often more subtle in radar imagery in TC tornado events than in classic Midwest tornadoes (Baker et al. 2009), which makes it difficult for forecasters to identify potentially tornadic storms. Furthermore, one of the most significant challenges in TC tornado outbreak prediction is distinguishing when a tropical system will trigger a prolific or non-prolific tornado outbreak event, which is linked to the dynamics from the tropical cyclone scale down to the mesoscale (Edwards 2012). Additionally, there is still much uncertainty about what specific environmental factors cause a landfalling TC to trigger a prolific tornado event while others result in non-prolific tornado outbreak events. Forecasting what part of the TCs environment is most conducive for a tornado outbreak is uncertain as well. By examining the different parameters and their specific values from the surface to 6 km, and surface to 1 km bulk wind difference (BWD), 1–6 km average relative humidity (RH), MLCAPE, MLECAPE, and MLECAPE P20 "to be defined below" for prolific and non-prolific events will increase the understanding of TC tornado outbreak environments for improved forecast predictions and resource protection.

Furthermore, it is well known that TC tornadoes are supercellular and occur with smaller values of CAPE than non-TC tornadoes. What we don't know is: how shear and entrainment might be different between high-end and low-end TC tornado outbreak events. Therefore, this research will compare the environmental characteristics through composite

plots and soundings of prolific TC tornadic events to non-prolific events of interest utilizing the NOAA climate reanalysis dataset (NCEP-DOE Reanalysis 2). Additionally, numerical simulations incorporate both composite soundings of prolific TCs, and non-prolific events for initial conditions using the non-hydrostatic Cloud Model 1 (CM1). Model simulations allowed us to determine differences in vertical velocity, surface and 1 km vorticity relating to shear and CAPE to help discriminate prolific TC tornadic events from non-prolific tornadic TCs. I hypothesize that an in-depth examination of individual storm parameters at the time of outbreak will provide new insight into distinguishing the dynamics of prolific and non-prolific tornadic outbreak TCs.

II. DATA AND METHODS

A. METHODS FOR REANALYSIS

Our focus was on the coastal regions of the southeast and mid-Atlantic states of the United States. This allowed for a more specialized dataset that focused on regions of the United States that are often impacted by TC tornado outbreak events. A compiled list of TC tornado outbreaks from (1979-2020) was used in this study by utilizing National Hurricane Center (NHC) tropical cyclone post-analysis reports (NOAA NHC, 2021). The dataset provides over 40 years and a total of 70 TC cases used to perform this research. Figure 1 provides a histogram plot to give a clear distribution of the dataset and show each TC tornado event organized by the total tornado outbreak number associated with each TC. With the max value of 118 tornadoes, the third quartile of 29 tornadoes, the 2nd quartile shows the median value of 13 tornadoes, the first quartile of 5 tornadoes, and a minimum value of 1 tornado for the events of interest. This allowed us to obtain a more extensive and even number of high-end and low-end events for this research. Data was then divided into the 70th percentile, with 23 high-end events producing 21 tornadoes or greater. Then the 30th percentile, which provided 23 low-end events that produced seven tornadoes or less.

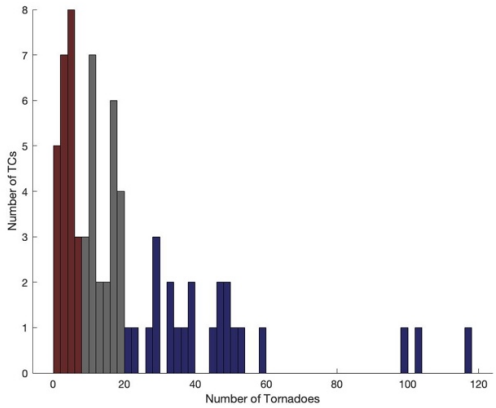

Red indicates 23 TCs with 7 tornados or less (low-end events). Blue indicates 23 TCs with 21 or greater tornadoes (high-end events).

Figure 1. TC Tornado Outbreak 1979–2020 Dataset

In addition to, the National hurricane Centers (NHC) Hurricane Best Track Data (HURDAT2), was utilized to identify the correct coordinates for each TC event. Best Track Data (HURDAT2) contains the name and best estimate of date, maximum winds, central pressure, location at 6-hourly intervals, and size of all known tropical cyclones and subtropical cyclones from post-analysis data (NOAA NHC, 2021). The data tracks a system from its initial tropical depression stage until it reaches the extra-tropical stage and is no longer classified as a tropical system (Schultz and Cecil 2009). For this research it was imperative to determine the exact location of the TC during the highest outbreak time within its lifespan. Furthermore, this research uses Storm Prediction Center's National Severe Weather Database Browser Online SeverePlot 3.0 to determine the approximate time and proximity to the center for when a given TC produced the highest tornado outbreak. SeverePlot 3.0 is:

> The official NWS data of tornadoes since 1950, along with hail and damaging convective winds since 1955. The data is derived from the Storm Data publication by National Weather Service, with review and processing conducted by the National Climatic Data Center and the Storm Prediction Center (NOAA SPC, 2021).

Tables 1 and 2 provide a detailed description of latitude and longitude coordinates, time, intensity, and TC category at the time of tornado outbreak well as the total number of tornadoes produced by each case for both data sets of high-end and low-end TC tornado events Figure 2 provides a visual representation of all high-end and low-end TC tornado events plotted at the time of the highest tornado outbreak. For both high-end and low-end events, the TCs show no geographic preference for the location of each event type.

Table 1. Tropical Cyclone Basic Information for High-End Events

LAT	LON	Tropical cyclone	YYYYMMDDHH	Category	Total tornadoes
33.4	77.9	Hurricane Dorian	2019090512	100kts Cat 2	21
28.4	94.8	Hurricane Alice	1983081800	95kts Cat 1	22
29.7	90.8	TS Isaac	2012082918	60kts TS	26
31.3	87.4	SD Allison	2001061200	25kts SD	28
25.8	96.8	Hurricane Allen	1980081000	110kts Cat 3	29
23.9	97.0	Hurricane Gilbert	1988091618	115kts Cat 4	29
30.3	95.2	Hurricane Ike	2008091312	55kts TS	33
32.8	79.5	TS Gaston	2004082912	65kts Cat 1	33
32.5	81.1	Hurricane David	1979090500	65kts Cat 1	34
31.3	85.0	TS Beryl	1994081612	30kts TD	37
32.8	79.1	Hurricane Isaias	2020080400	80kts Cat 1	39
31.0	92.4	TS Danny	1985081600	50kts TS	39
33.9	78.8	TS Florence	2018091500	60kts TS	44
30.4	91.6	TS Lee	2011090500	35kts TS	46
30.6	89.0	Hurricane George	1998092900	50kts TS	47
28.5	90.3	Hurricane Cindy	2005070600	65kts Cat 1	48
29.8	91.4	TS Gustav	2008090118	60kts TS	49
33.9	87.2	TD Fay	2008082612	20kts TD	50
28.8	96.8	TS Harvey	2017082800	35kts TS	52
35.6	88.0	TD Katrina	2005083012	30kts TD	59
34.7	92.5	TS Rita	2005092512	25kts TD	98
31.0	84.6	TS Frances	2004090700	35kts TS	103
28.9	88.2	Hurricane Ivan	2004091600	110kts Cat 3	118

Table 2. Tropical Cyclone Basic Information for Low-End Events

LAT	LON	Tropical cyclone	YYYYMMDDHH	Category	Total tornadoes
36.7	77.7	Hurricane Isabel	2003091900	65kts TS	1
33.7	75.4	TS Gustav	2002091012	45kts TS	1
30.5	81.6	TS Tammy	2005100600	45kts TS	1
28.8	94.8	TS Humberto	2007091300	55kts TS	1
31.5	79.3	TS Hanna	2008090600	60kts TS	1
40.2	74.3	TS Fay	2020071100	35kts TS	1
24.9	81.3	TS Dennis	1981081700	35kts TS	2
33.2	76.0	Hurricane Gloria	1985092700	90kts Cat 2	2

LAT	LON	Tropical cyclone	YYYYMMDDHH	Category	Total tornadoes
28.0	89.2	TS Hanna	2002091400	50kts TS	2
30.4	86.7	TD Ten	2007092200	25kts TD	2
31.7	78.8	Hurricane Hugo	1989092200	120kts Cat 4	3
30.1	87.5	TS Arlene	2005061118	50kts TS	3
28.6	87.1	TS Nestor	2019101900	50kts TS	3
29.5	94.3	Hurricane Chantal	1989080112	70kts Cat1	4
30.1	80.7	TS Beryl	2012052800	60kts TS	4
29.1	85.9	TS Alberto	2018052812	50kts TS	4
26.7	97.6	Hurricane Hanna	2020072600	75kts Cat 1	5
28.2	92.9	Hurricane Bonnie	1986062600	70kts Cat 1	5
29.1	95.0	Hurricane Jerry	1989101600	75kts Cat 1	5
34.6	75.3	Hurricane Bob	1991081800	70kts Cat1	5
29.5	86.3	TS Barry	2001080600	60kts TS	6
26.4	97.2	Hurricane Dolly	2008072318	75kts Cat 1	7
27.2	96.2	TS Erin	2007081606	35kts TS	7

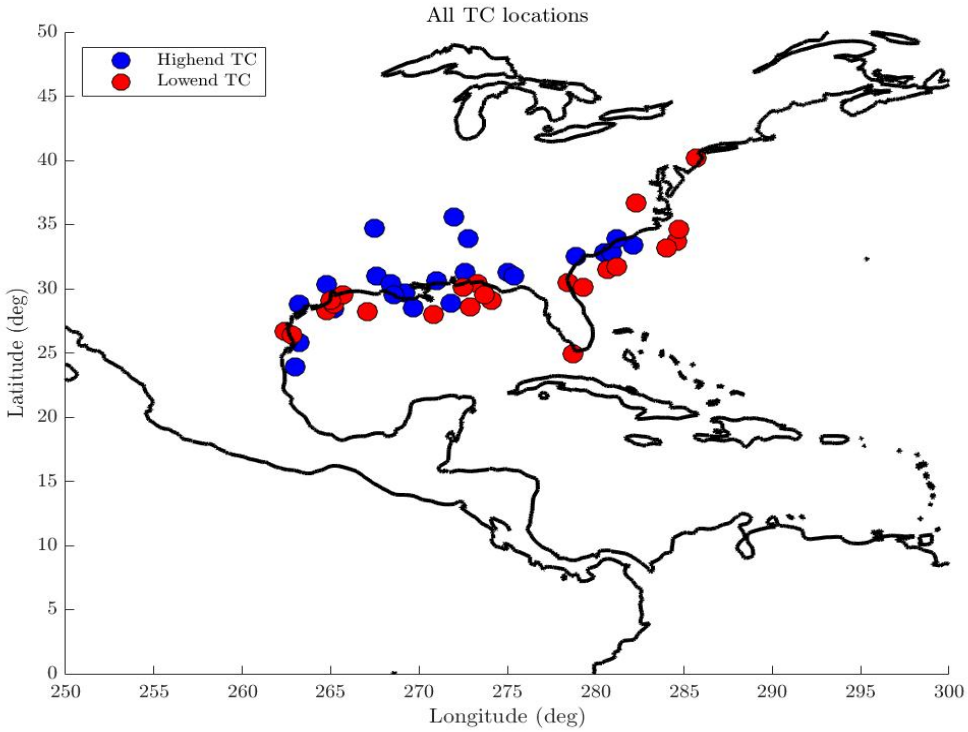

Figure 2. TC Center Location at Time of Tornado Outbreak

Furthermore, to examine each TC tornado events environmental parameters, NOAA climate reanalysis dataset (NCEP-DOE Reanalysis 2) data from the National Center for Environmental Prediction (NCEP) was used as the reanalysis dataset of choice for this research. NCEP-DOE Reanalysis 2 uses "a state-of-the-art analysis system to perform data assimilation using past data from 1979 through the previous year. A large subset of this data is available from NOAA Physical Science Laboratory (PSL) in four times daily format and as daily averages" (NOAA PSL, 2021).

The following variables were used in netcdf format for this study: air temperature, geopotential height, relative humidity, u-wind, and v-wind components. With a spatial coverage of 2.5-degree latitude x 2.5-degree longitude global grid (144x73), 90N - 90S, 0E - 357.5E (NOAA PSL, 2021). Reanalysis data was ingested into local computer programs for further investigation and then used to produce storm following composite plots to analyze differences in surface to 1 km, surface to 6 km bulk wind difference (BWD), 1–6 km average relative humidity (RH), CAPE for high-end and low-end TC events. Furthermore, composite plots allowed us to determine where we would obtain our composite proximity soundings to compare differences for both high-end and low-end TC tornado environments and used as initial conditions for model simulations. We generated composites by selecting data within a 10 by 10 analysis grid point box that was modified to be proportional; to storm scale (i.e., 10 by 10 points for small and large storms relative to total storm scale or constant spacing) centered at the location of the TC at the time of the outbreak (usually near the TC landfall time). We then averaged these analysis boxes over all events to generate the composites. MLCAPE was computed by first vertically interpolating data onto a vertical grid with a 100 m grid spacing. We then adiabatically lifted all parcels from all grid points below 1 km using the method outlined by Peters et al. (2021). The buoyancies for each of these parcels were then computed, averaged over all parcels, and the resulting averaged buoyancy profile was vertically integrated to obtain MLCAPE.

MLECAPE followed the same strategy, but with an assumed fractional entrainment rate of 5×10^{-5} m^{-1}, using the entrainment procedures introduced in (Peters et al. 2021). A second MLECAPE (hereafter MLECAPE P20) formula was used from Peters et al. (2020),

wherein the fractional entrainment rate was diagnosed from the vertical wind shear profile. In principle, the MLECAPE P20 formula should most accurately depict updraft vertical velocities, as was shown in Peters et al. (2020) who compared the performances of MLCAPE, MLECAPE, and MLECAPE P20 to the output from numerical simulations. CAPE was computed within the analyses boxes of individual events first, and then averaged to make composites.

B. MODEL SETUP

For this research simulations used Cloud Model 1 (CM1, Bryan and Fritsch 2002), to demonstrate the differences of tornadic environments from composite soundings of both high-end and low-end TC tornado events. CM1 is designed specifically to simulate deep convective processes. It features a non-hydrostatic dynamical core with an acoustic time-stepping procedure to handle sound waves.

Model simulations used a grid/time step resolutions in a 100 km × 100 km box, with a 100 m horizontal and 100 m vertical grid spacing resolution. Table 3 provides a complete model setup of all CM1 parameters used in our simulation. The input soundings for CM1 were constructed from a proximity sounding of the location of highest tornadic activity for high-end events. Additionally, the same approach was used for the proximity sounding of the highest tornadic activity for low-end-events.

Table 3. CM1 Model Configuration

Attribute	**Value/Setting**	**Notes**
Fully Compressible	Yes	
Horizontal Grid Spacing	100 m	
Vertical Grid Spacing	100 m	
Vertical Coordinate	Height (m)	
Number of x and y Points	100 x 100	
Vertical Points	150	
Top/Bottom LBCs	Free-slip	
North/South LBCs	Open-radiative	Durran and Klemp (1983)

Attribute	Value/Setting	Notes
East/West LBCs	Open-radiative	Durran and Klemp (1983)
Microphysics	Morrison	Morrison et al. (2009)
Diffusion	6^{th} order	
Subgrid Turbulence	TKE	
Rayleigh Dampening	Yes	
Dissipative Heating	Yes	
2^{nd} and 6^{th} Order Coef.	75-.04	
Longwave Radiation	None	
Shortwave Radiation	None	
Surface Layer	None	
Boundary Layer Physics	None	
Cumulus Parameterization	None	

C. METHODS FOR ANALYSIS

The strategy for the model simulations was to take two composites: one representing the high-end TC tornado environments and one representing low-end TC tornado environments, to initialize the model. Two model simulations were run utilizing the two different sounding environments. Vertical velocity *w* differences were investigated between high-end and low-end TC tornado environments. Additionally, we investigated how surface and 1 km vorticity was different between both soundings. Nowotarski et al. (2011) used this approach, who showed that using this method can show tornado potential when incorporated into model simulations.

THIS PAGE INTENTIONALLY LEFT BLANK

III. RESULTS

A. STORM FOLLOWING COMPOSITES

Composites for all the high-end and low-end events that are storm-centered at the exact day and time of TC tornado outbreak were produced to display surface to 6 km BWD and can be seen in Figure 3. We observed from both composite plots a rather large spatial variability of BWD. High-end composites for surface to 6 km result in higher magnitude BWD in the right-front quadrant in relation to the storm center which was found by lowest 1 km geopotential height contour. For surface to 6 km composite plots, values show greater than 11 (m/s) of BWD. Research shows that surface to 6 km BWD is important to the development of supercells. The deeper layer shear surface to 6 km helps to increase low-level storm-relative flow, which allows supercell updrafts to become wider and thus have a higher probability of supercellular storm mode (Peters et al. 2019). The shear is more maximized in the storm composite's right quadrant, contributing to the proximity of where tornado outbreaks typically occurred. Furthermore, the increased deep-layer shear in the right quadrant of the composite results from a baroclinic interaction with an associated upper-level trough at the time of the outbreak, which helped generate enhanced vertical wind shear producing an environment favorable for the development of tornadoes. This process was determined by subjective analyses of the 500 mb geopotential height gradient positions and 850 mb temperature relative to the TC location. We found 17 of the 23 high-end events showed this particular synoptic setup during the time of the tornado outbreak. Conversely, we found 5 of the 23 low-end events to show this particular synoptic setup.

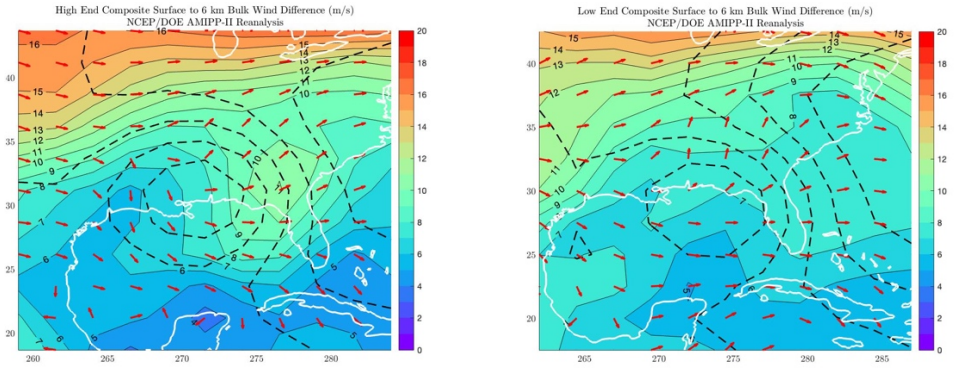

Left panel displays high-end composite plots of surface to 6 km BWD . Right panel displays low-end composite plots of surface to 6 km BWD. Shading colors depict magnitude of BWD (m/s). Black contours provide composite storm center in 1 km geopotential height. Red vectors depict the direction of wind shear. X-axis depicts longitude (deg) and y-axis depicts latitude (deg).

Figure 3. Storm Following Surface to 6 km Bulk Wind Difference Composites

To show the differences in the high-end and low-end composites we generated a comparison composite difference plot which can be seen in Figure 4. We found that the high-end composite produced greater than 4 (m/s) of BWD in the right quadrant of the storm following composite in relation to the average storm center.

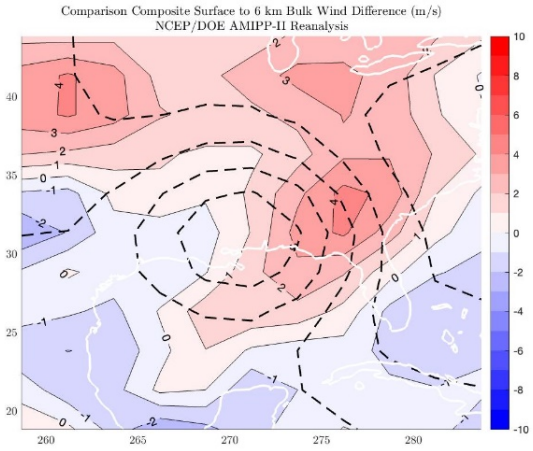

Plot displays comparison composite plot of surface to 6 km BWD. Shading colors depict difference in magnitude of BWD (m/s). Black contours provide composite storm center in 1 km geopotential height. X-axis depicts longitude (deg) and y-axis depicts latitude (deg).

Figure 4. Comparison Composite Surface to 6 km Bulk Wind Difference

Similar to the surface to 6km BWD composites we produced plots to show surface to 1km BWD for all the high-end and low-end events that are storm centered at the exact day and time of TC tornado outbreak and can be seen in Figure 5. We found a similar spatial distribution as what was observed with surface to 6 km BWD with a maximum in the right quadrant. However, the lower-level surface to 1 km BWD and deeper layer surface to 6 km BWD shear have separate dynamical implications for how storms evolve. Particularly the lower layer shear helps determine whether a TC will produce strong supercells and potentially tornadoes (Coffer and Parker 2017). These different layers can vary independently, so it is essential to incorporate both for this research. High-end composites for surface to 1 km result in higher magnitude BWD in the right quadrant relative to the composite storm center, with BWD values generally around 7 (m/s). Additionally, the low-end composite resulted in increased BWD in the right quadrant yet only yielded BWD values of 4.5 (m/s). We also found the wind shear direction vectors normalized by the magnitude with a rather cyclonic change in the shear direction around the center of the high and low-end composite TCs.

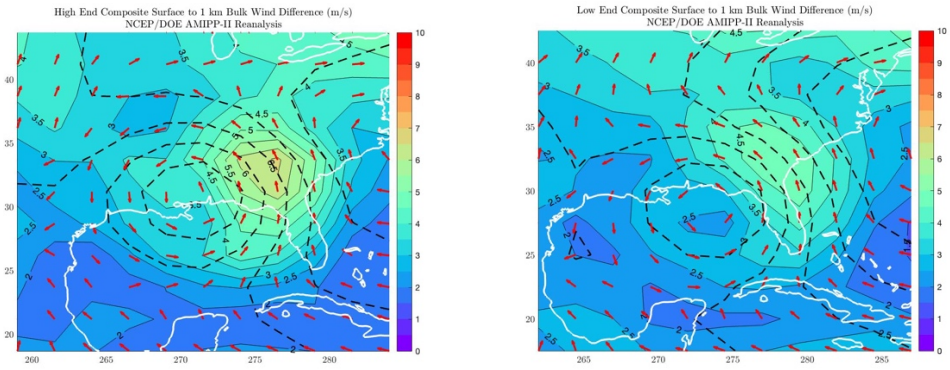

Left panel displays high-end composite plots of surface to 1 km BWD. Right panel displays low-end composite plots of surface to 1 km BWD. Shading colors depict magnitude of BWD (m/s). Black contours provide composite storm center in 1 km geopotential height. Red vectors depict the direction of wind shear. X-axis depicts longitude (deg) and y-axis depicts latitude (deg).

Figure 5. Storm Following Surface to 1 km Bulk Wind Difference Composites

The comparison high-end minus low-end difference plot for surface to 1 km BWD seen in Figure 6 allowed us to show a definitive difference in low-level wind shear between the high-end and low-end dataset. Red shading indicates that the high-end composite had the highest values of low-level wind shear, with the highest difference on the right quadrant of the BWD comparison plot with values greater than 1.5 (m/s) on average.

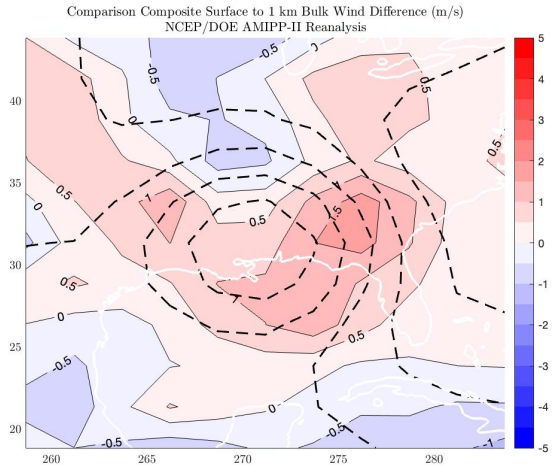

Plot displays comparison composite plot of surface to 1 km BWD. Shading colors depict difference in magnitude of BWD (m/s). Black contours provide composite storm center in 1km geopotential height. X-axis depicts longitude (deg) and y-axis depicts latitude (deg).

Figure 6. Comparison Composite Surface to 1 km Bulk Wind Difference

To investigate the amount of moisture in the lower to middle atmosphere, we obtained 1–6 km average relative humidity (RH) plots to observe the difference in the high-end and low-end composite, as shown in Figure 7. This layer of the atmosphere is particularly important in developing deep convection and gives insight into how much moisture is in the environment. Also, this particular level has been shown to have the biggest impact in terms of entrainment. Similar to low-level and deep-shear plots, as each system moved into the mid-latitudes, it allowed for a rather large spatial variability. We found that both the high-end and low-end composites show the highest values offset from the composite storm center with the highest values of 1–6 km average relative humidity (RH) over the right quadrant. Furthermore, high values of 1–6 km average relative

humidity (RH) seem to correspond similarly to the proximity of where tornado outbreaks occur in TCs.

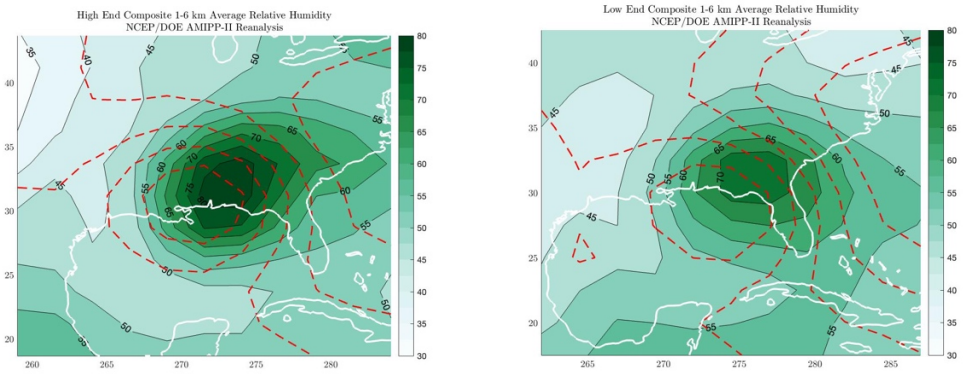

Left panel displays high-end composite plots of 1–6 km Average Relative Humidity. Right panel displays low-end composite plots of 1–6 km Average Relative Humidity. Shading colors depict relative humidity. Red contours provide composite storm center in 1 km geopotential height. X-axis depicts longitude (deg) and y-axis depicts latitude (deg).

Figure 7. Storm Following 1–6 km Average Relative Humidity Composites

By comparing high-end and low-end cases, we found a definitive difference in the quantity of 1–6 km average relative humidity (RH). With RH values greater than 10 percent for high-end composites as opposed to the low-end composite events. The highest difference can easily be observed from the right-center to most of the right quadrant and can be seen in Figure 8, highlighted by subtracting the low-end from the high-end.

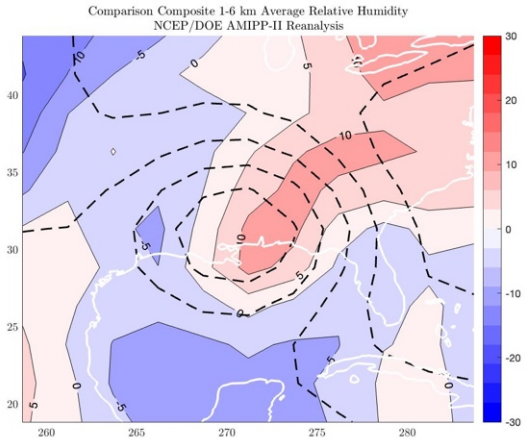

Plot displays comparison composite plot of 1–6 km Average Relative Humidity. Shading colors depict the difference in relative humidity Black contours provide composite storm center in 1 km geopotential height. X-axis depicts longitude (deg) and y-axis depicts latitude (deg).

Figure 8. Comparison Composite 1–6 km Average Relative Humidity

Again, by taking the same approach to obtaining composite plots for the previously mentioned variables, we also produced composite plots for 0–1 km mean layer convective potential energy (MLCAPE) shown in the top two panels of Figure 9. We found a less pronounced difference in the distribution of MLCAPE between the high-end and low-end events. In fact, areas in the right-front quadrant that resulted in higher values of low-level, deep-level BWD and 1–6 km average relative humidity (RH) seemed to not correspond with the same proximity of the distribution of MLCAPE. Additionally, we found high values of MLCAPE over the right quadrant for the low-end vice high-end composites shown by the top panel in Figure 10. This result seems to be contrary to what we had expected, given that intuition suggests that larger MLCAPE equates to stronger storms and greater potential for tornadoes. This shows that MLCAPE may not be the main environmental factor to be used in distinguishing prolific and non-prolific tornado outbreaks regarding TCs. This result is consistent with analyses of non-TC tornadoes, which show that various different measures of CAPE are poor discriminators between tornadic and nontornadic storms (Coffer et al. 2019).

Furthermore, we also investigated the role of entrainment and its impact on 0–1km mean layer convective potential energy using MLECAPE and a new method for calculating

0–1km mean layer MLECAPE P20. The two middle panels in Figure 9 show MLECAPE differences between high-end and low-end cases with similar distribution as regular MLCAPE but with dampened values due to entrainment above the EIL being a factor. However, MLECAPE P20 incorporates a new formula to improve predictions of maximum *w* over prior MLECAPE derived formulas (Peters et al. 2020a). This allowed higher values of MLECAPE P20 over the right quadrant where we found higher values of low-level, deep-level BWD and 1–6 km average relative humidity (RH). The bottom panel of Figure 10 shows the comparison composites of both high-end and low-end MLECAPE P20. Again we found that the difference shows higher MLECAPE P20 over the right quadrant for high-end events compared to low-end composites. This result shows that using MLECAPE P20 may be a better metric for determining the buoyancy of supercells than regular MLCAPE when investigating the TC tornadic outbreak potential environment. Ultimately, the entrainment rate is more accurate where it shows more correspondence to regions of higher tornadic activity. The difference plots show how it minimizes the difference between the two composites. When entrainment is taken into account updrafts are more similar in buoyancy shown by the bottom panel of Figure 10, compared to the top panel which shows the MLCAPE comparison difference to be higher in the low-end events, but once we take entrainment into account there is less of a difference.

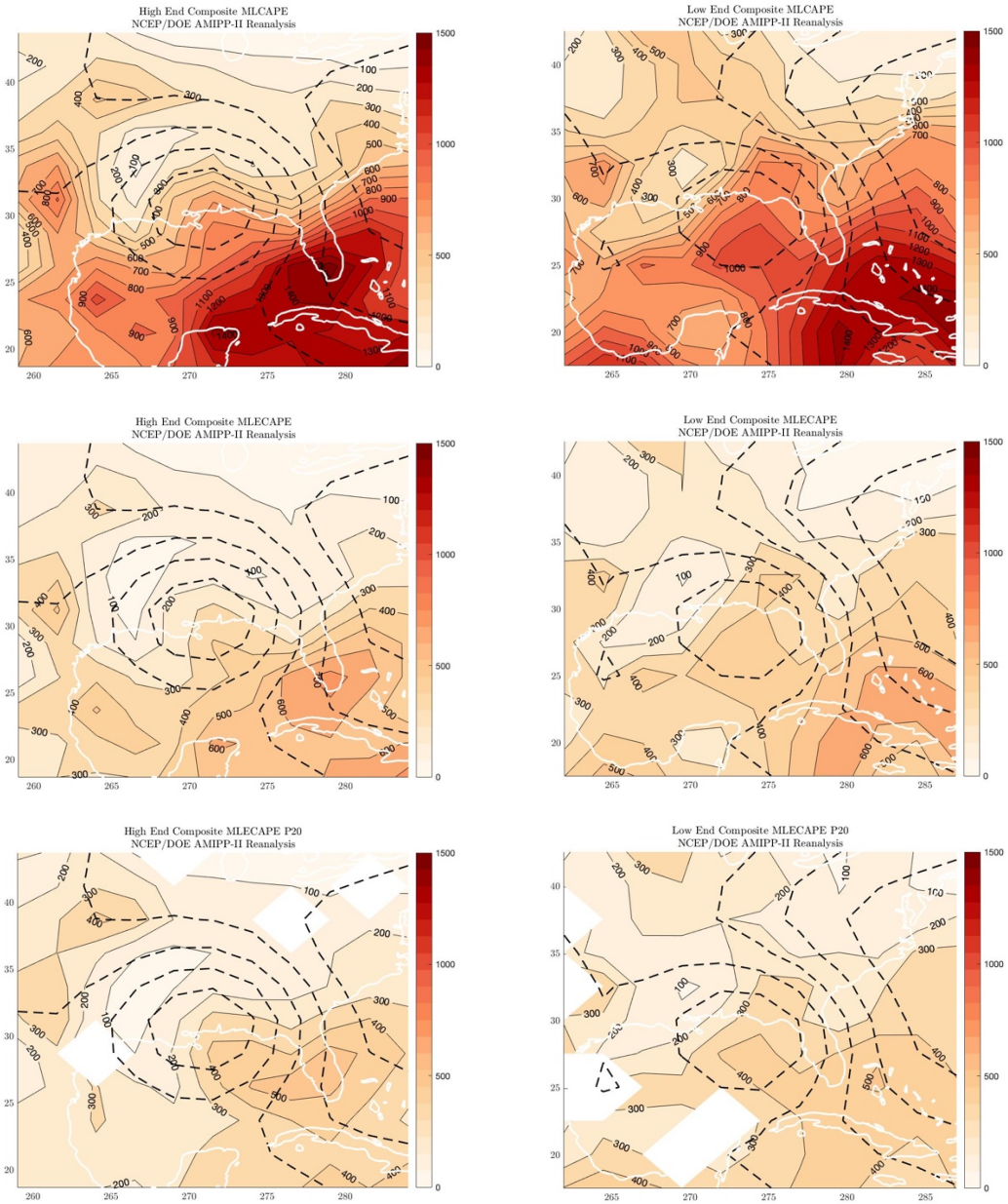

Left panel displays high-end composite plots MLCAPE, MLECAPE, MLECAPE_P20. Right panel displays low-end composite plots MLCAPE, MLECAPE, MLECAPE_P20. Shading colors depict CAPE values in units of Joules/kg. Black contours provide composite storm center in 1km geopotential height. Red vectors depict the direction of wind shear. X-axis depicts longitude (deg) and y-axis depicts latitude (deg).

Figure 9. Storm Following MLCAPE, MLECAPE, MLECAPE P20 Composites

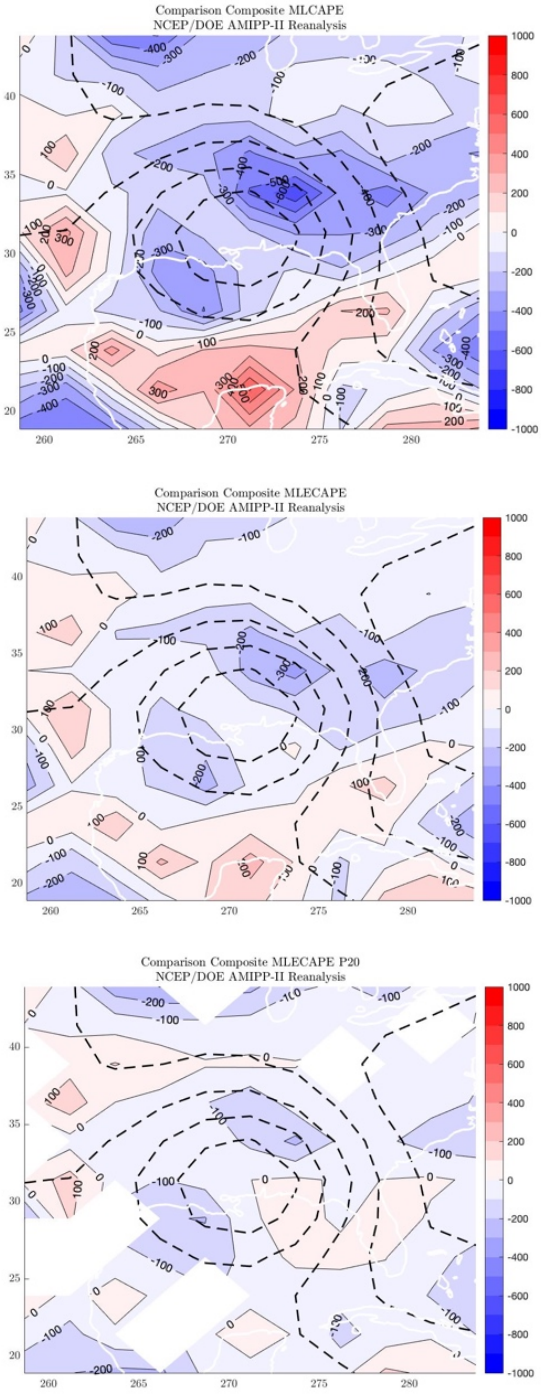

Plots display comparison composite plot of MLCAPE, MLECAPE, MLECAPE_P20. Shading colors depict difference in MLCAPE, MLECAPE. Black contours provide composite storm center in 1km geopotential height. X-axis depicts longitude (deg) and y-axis depicts latitude (deg).

Figure 10. Comparison Composite MLCAPE, MLECAPE, MLECAPE P20

B. COMPOSITE SOUNDING PROFILES

Utilizing the storm following composite plots allowed us to develop a strategy to determine where relative to the center of the composite storm location, we obtained our composite soundings to compare high-end and low-end. We found that the MLCAPE values were slightly higher than we observed with composite plots when deriving composite soundings for high-end and low-end events. This is likely because composite plots MLCAPE were produced by averaging MLCAPE for each event. In contrast, composite soundings were produced by averaging each variable to compute MLCAPE separately before producing the given composite soundings. However, both high-end and low-end composite soundings show slightly different values but roughly the same order of magnitude for both. Furthermore, we found both composite soundings have similar values of MLCAPE, with the low-end composite observing slightly larger values seen in Figure 13. However, when observing the midlevel dewpoint and environmental temperature difference, the high-end composite sounding presented in Figure 11 showed lower dewpoint depression values when compared to the low-end composite sounding. Additionally, Figure 12 presents the composite sounding wind profiles. We found the high-end composite wind profile to show the most significant low-level and deep-level wind shear compared to the low-end composite wind profile shown in Figure 14. These two unique soundings resulted in four main parameters for initial conditions of model simulations on a surface to 20 km height grid of potential temperature, mixing ratio, u-wind, and v-wind components.

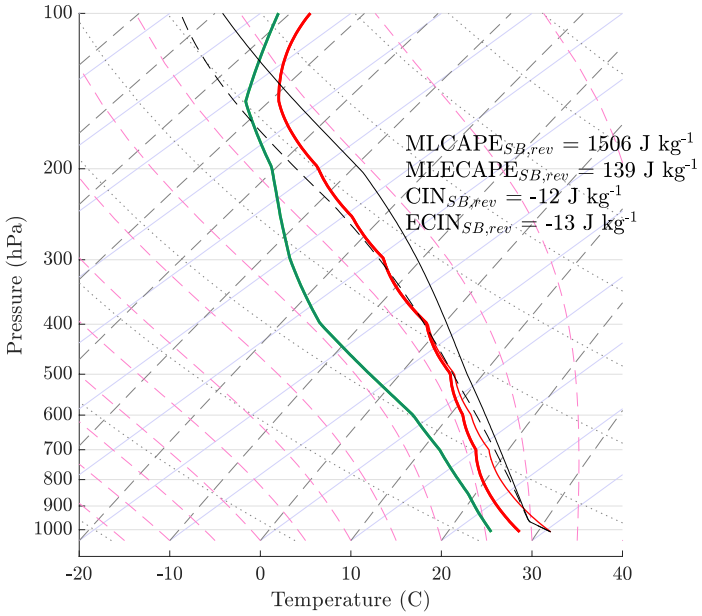

Skew T log p temperature and moisture profile. Solid red line represents environmental temperature. Thinner red line represents virtual temperature of environment. Green line represents dewpoint. Solid black line shows the temperature of a buoyant air parcel. Titled solid lines are isotherms, long dashed lines are moist adiabats, and short dashed lines are dry adiabats.

Figure 11. High-End Composite Environmental Sounding

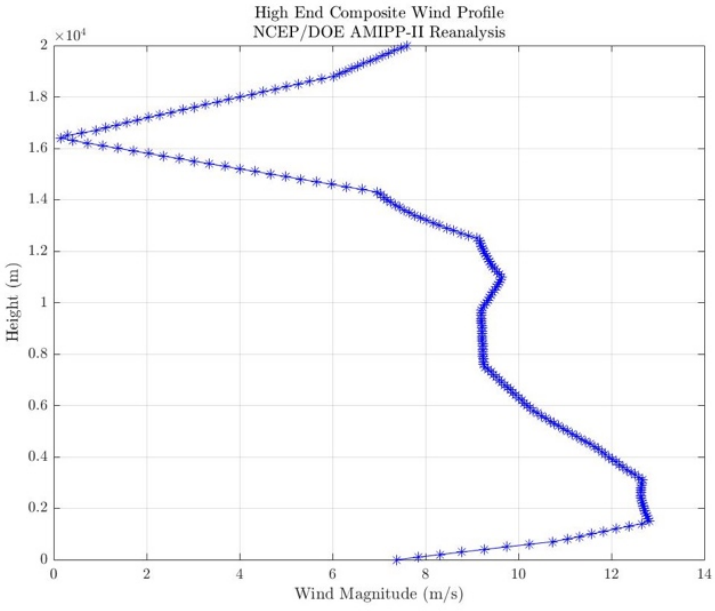

Figure 12. High-End Composite Environmental Wind Profile

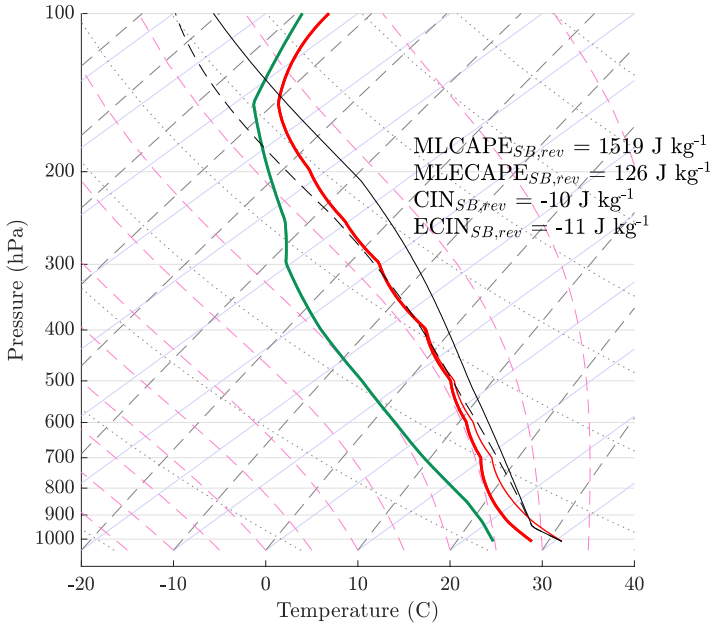

Skew T log p temperature and moisture profile. Solid red line represents environmental temperature. Thinner red line represents virtual temperature of environment. Green line represents dewpoint. Solid black line shows the temperature of a buoyant air parcel. Titled solid lines are isotherms, long dashed lines are moist adiabats, and short dashed lines are dry adiabats.

Figure 13. Low-End Composite Environmental Sounding

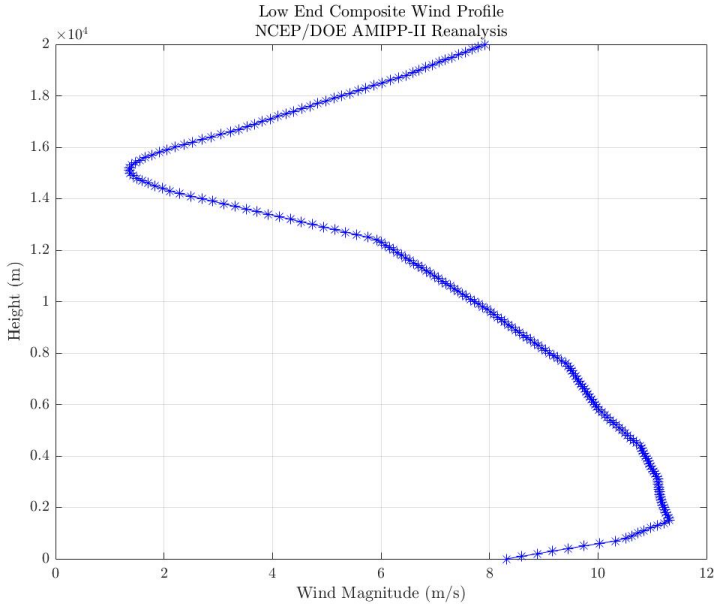

Figure 14. Low-End Composite Environmental Wind Profile

C. MODEL SIMULATIONS

The composite soundings described in the previous sub-section were each used to initialize a CM1 simulation. First, the initial conditions everywhere in the model domains were set to these soundings. Random temperature perturbations were added to the initial conditions with maximum amplitudes of +/- 0.25 K to drive the development of turbulent eddies. A uniform surface flux was applied to the lower boundary for 1 hour to spin-up a turbulent boundary layer. The sensible heat flux was 0.03 W m-2, and the latent heat flux was set to 1x10-3 W m-2. At 1 hour, the surface flux over a Gaussian shaped region with a radius of influence of 5 km and a maximum was increased by a maximum amplitude factor of 20. The purpose of this enhanced flux was to generate deep convective updrafts.

In both simulations, a supercell-like updraft developed over the enhanced flux region, and persisted for approximately 1 hour. In both simulations, this updraft featured a classic "comma" shape in simulated radar reflectivity, along with a hook-echo. As shown in Figure 15, we found a definitive difference in max vertical velocity between both cases. For the high-end, a large increase in vertical velocity *w* is apparent between 0.5 and 1 hour, with a vertical velocity *w* maximum of 60 (m/s) at 12 km in height. In contrast, we found the highest vertical velocity after 1 hour for the low-end composite sounding and a lower vertical velocity of less than 50 (m/s) at generally the same height as the high-end. Furthermore, we found a decisive difference in the cloud top height, with the high-end showing the highest cloud top height maximum greater than 20 km reached between 1 hour and 1.5 hours. This corresponds to the higher vertical velocity *w* seen in the high-end versus the low-end composite sounding. Vorticity at the surface was investigated with the high-end resulting in a more significant increase between 1 and 2 hrs. However, interestingly, 1 km vorticity between high-end and low-end composite soundings showed minimal variation of the magnitude throughout the simulation duration.

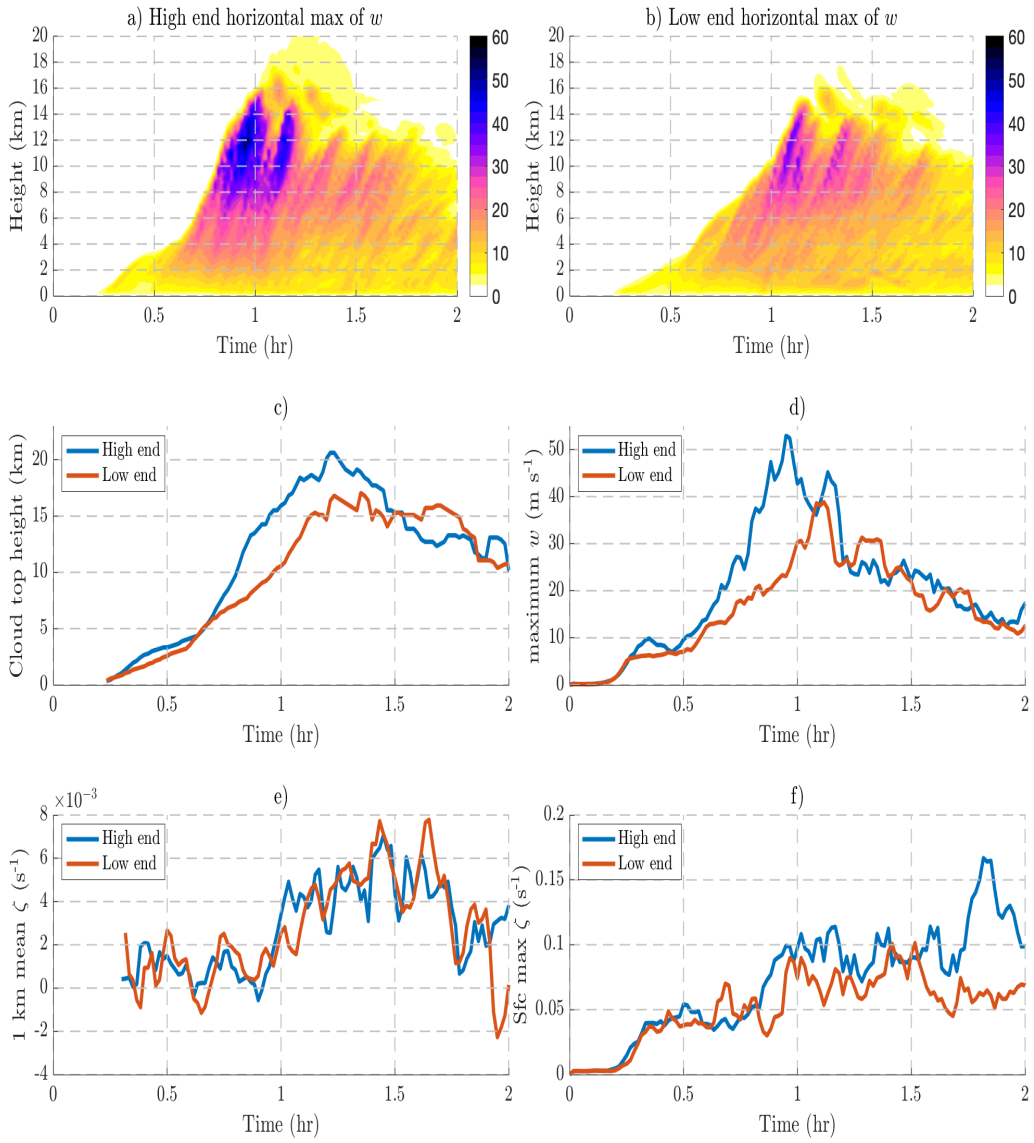

Time series displays vertical velocity, cloud height, maximum vertical velocity, 1km and surface vorticity for high-end and low-end. Panels a and b: The x-axis is time in hours. The y-axis is vertical velocity for both high-end and low-end. Panel c: The x-axis is time in hours. The y-axis is cloud height (km) for both high-end and low-end. Panel d: The x-axis is time in hours. The y-axis is maximum vertical velocity for high-end and low-end. Panels e and f: The x-axis is time in hours. 1 km and surface vorticity for high-end and low-end.

Figure 15. Vertical Velocity and Vorticity Time Series

IV. SUMMARY AND CONCLUSIONS

One of the most significant challenges in TC tornado outbreak prediction is distinguishing between when a tropical system will become a prolific or non-prolific tornado outbreak event, specifically, and what environmental factors are involved. As well as forecasting what part of the TCs environment is most conducive for a tornado outbreak. Furthermore, we don't know how shear and entrainment might differ between high-end and low-end TC tornado outbreak events. This research paper investigates environmental parameters and their differences regarding a composite of 23 high-end prolific and 23 low-end non-prolific TC tornado events to address uncertainties. The following environmental parameters examined include surface to 6 km bulk wind difference (BWD), surface to 1 km bulk wind difference (BWD), 1–6 km average relative humidity (RH), MLCAPE, MLECAPE, and MLECAPE P20. The hypothesis considered an in-depth examination of individual storm parameters at the time of outbreak will provide new insight into distinguishing the dynamics of prolific and non-prolific tornadic outbreak TCs.

To test the validity of our hypothesis, we compared the differences in both the magnitude and spatial distribution of each of the parameters. This allowed us to address our research question of how shear and entrainment differed between high-end prolific and low-end non-prolific events. Then from the various parameters investigated, we found where relative to the composite storm center the largest magnitude of the values and their differences. Then we obtained our proximity soundings for both high-end and low-end cases. From our two proximity soundings, we derived four main parameters for initial conditions of model simulations on a surface to 20 km height grid of potential temperature, mixing ratio, u-wind, and v-wind components. The results found from composite parameter comparisons and simulation model runs are explained as follows:

- Both event types featured regions of locally enhanced 0–6 km BWD in their right-front quadrants. Maximum values in the high-end cases were 11 (m/s) when compared to 7 (m/s) in the low-end cases. The values in the high-end cases were also statistically more significant in this right-front region than

those in the low-end cases. This suggests that prolific tornado producing TC events feature more significant deep-layer shear than non-prolific events.

- Similar patterns of enhanced 0–1 km BWD were present in both event types in the right-front quadrant. Once again, maximum 0–1 km BWDs were larger for high-end events, peaking near 7 (m/s), whereas they only peaked near 4.5 (m/s) in the low-end events. These differences were statistically significant, suggesting that high-end TC events feature larger low-level shear than low-end TC events.

- From the 23 high-end TC tornado events, we found 17 events showed a baroclinic interaction with an associated upper-level trough at the time of the outbreak. This process was determined by subjective analyses of the 500 mb geopotential height gradient positions and 850 mb temperature relative to the TC location. Which helped generate increased deep layer shear in the right quadrant, enhancing an environment favorable for the development of tornado outbreaks.

- To investigate the amount of moisture in the lower to the middle atmosphere, we obtained 1–6 km average relative humidity (RH) plots to observe the difference in the high-end and low-end composite. Similar to low-level and deep-shear plots, we found a rather large spatial variability with values greater than 10 percent over the right quadrant for high-end events.

- Both event types we investigated MLCAPE over the right quadrant. With the slightly higher values of MLCAPE found over the right quadrant for low-end events. Additionally, we found less of a definitive difference between the two. This result seems to be contrary to what we had expected. This shows that MLCAPE may not be the main environmental factor to be used in distinguishing prolific and non-prolific tornado outbreaks regarding TCs.

- Similarly, we investigated MLECAPE P20, which incorporates a new formula to improve predictions of maximum *w* over prior MLECAPE

derived formulas. This allowed higher values of MLECAPE P20 over the right quadrant in contrast to MLECAPE, where we found higher values of low-level, deep-level BWD and 1–6 km average relative humidity (RH). This result shows that using MLECAPE P20 may be a better metric for determining buoyancy than regular MLCAPE and MLECAPE when investigating the TC tornadic outbreak potential environment. Also, it shows more correspondence to the proximity of tornado outbreaks; the comparison difference plots show how it minimizes the difference between both composite cases.

- For model simulations, we found a definitive difference in max vertical velocity between both cases. For the high-end, a vertical velocity *w* maximum of 60 (m/s) at 12 km in height. In contrast, the low-end composite, we found a lower vertical velocity of less than 50 (m/s) at generally the same height as the high-end. Vorticity at the surface was investigated with the high-end resulting in a greater increase in the magnitude with time. However, 1 km vorticity showed very minimal variation between both soundings throughout the model simulation.

The findings from the study can be applied to improve forecasting techniques to identify different environmental factors in a prolific TC tornado outbreak event from a non-prolific outbreak, allowing for early preparation to protect the public and improved resource protection programs. More focus on environmental factors such as strong low-level and deep-layer shear and the propensity to produce tornadic outbreaks would be beneficial. Furthermore, findings in this research suggest less focus should be applied to CAPE, and specifically the typical used indices that depend on CAPE, such as the significant tornado parameter. Additionally, the effects of entrainment and the utility of MLECAPE P20 may be a better metric for distinguishing tornadic from non-tornadic environments. Future work will focus on the effects of entrainment, with more simulations and dynamical analysis to understand the differences.

THIS PAGE INTENTIONALLY LEFT BLANK

LIST OF REFERENCES

Baker, A. K., M. D. Parker, and M. D. Eastin, 2009: Environmental Ingredients for Supercells and Tornadoes within Hurricane Ivan. *Weather Forecast.*, **24**, 223–244, https://doi.org/10.1175/2008WAF2222146.1.

Bryan, G. H., and J. M. Fritsch, 2002: A Benchmark Simulation for Moist Nonhydrostatic Numerical Models. *Mon. Weather Rev.*, **130**, 2917–2928, https://doi.org/10.1175/1520-0493(2002)130<2917:ABSFMN>2.0.CO;2.

Caulfield, S. P., 2018: The Influence Of Boundary-Layer Shear And Static Stability On Low-Level Vertical Accelerations In A Supercell. Monterey, CA; Naval Postgraduate School, https://calhoun.nps.edu/handle/10945/61328 (Accessed October 6, 2021).

Coffer, B. E., and M. D. Parker, 2017: Simulated Supercells in Nontornadic and Tornadic VORTEX2 Environments. *Mon. Weather Rev.*, **145**, 149–180, https://doi.org/10.1175/MWR-D-16-0226.1.

Coffer, B. E., and M. D. Parker, R. L. Thompson, B. T. Smith, and R. E. Jewell, 2019: Using Near-Ground Storm Relative Helicity in Supercell Tornado Forecasting. *Weather Forecast.*, **34**, 1417–1435, https://doi.org/10.1175/WAF-D-19-0115.1.

Edwards, R., 2012: Tropical Cyclone Tornadoes: A Review of Knowledge in Research and Prediction. 61.

Gentry, R. C., 1983: Genesis of Tornadoes Associated with Hurricanes. *Mon. Weather Rev.*, **111**, 1793–1805, https://doi.org/10.1175/1520-0493(1983)111<1793:GOTAWH>2.0.CO;2.

Grazulis, T. P., 1990: Significant tornadoes.....A 107 year perspective. *J. Wind Eng. Ind. Aerodyn.*, **36**, 131–151, https://doi.org/10.1016/0167-6105(90)90299-R.

Houston, A. L., R. L. Thompson, and R. Edwards, 2008: The Optimal Bulk Wind Differential Depth and the Utility of the Upper-Tropospheric Storm-Relative Flow for Forecasting Supercells. *Weather Forecast.*, **23**, 825–837, https://doi.org/10.1175/2008WAF2007007.1.

Moncrieff, M., and M. Miller, 1976: Dynamics and Simulation of Tropical Cumulonimbus and Squall Lines. *Q. J. R. Meteorol. Soc.*, **102**, 373–394, https://doi.org/10.1002/qj.49710243208.

NCAR, 2021: Frequently Asked Questions about CM1. http://www2.mmm.ucar.edu/people/bryan/cm1/faq.html, accessed September 2021.

NOAA, 2021: Weather Glossary: M's. https://forecast.weather.gov/glossary.php?letter=m, accessed 21 September 2021.

NOAA NHC, 2021: Data Archive. https://www.nhc.noaa.gov/data/#tcr, accessed 21 September 2021.

NOAA PSL, 2021: NCEP-DOE AMIP-II Reanalysis. https://psl.noaa.gov/data/gridded/data.ncep.reanalysis2.pressure.html, accessed 21 September 2021.

NOAA SPC, 2021: Online SeverePlot 3.0. https://www.spc.noaa.gov/climo/online/sp3/, accessed 21 September 2021.

Nowotarski, C. J., P. M. Markowski, and Y. P. Richardson, 2011: The Characteristics of Numerically Simulated Supercell Storms Situated over Statically Stable Boundary Layers. *Mon. Weather Rev.*, **139**, 3139–3162, https://doi.org/10.1175/MWR-D-10-05087.1.

Peters, J. M., C. J. Nowotarski, and H. Morrison, 2019: The Role of Vertical Wind Shear in Modulating Maximum Supercell Updraft Velocities.

Peters, J. M., H. Morrison, C. J. Nowotarski, J. P. Mulholland, and R. L. Thompson, 2020a: A Formula for the Maximum Vertical Velocity in Supercell Updrafts. *J. Atmospheric Sci.*, **77**, 3747–3757, https://doi.org/10.1175/JAS-D-20-0103.1.

Peters, J. M., C. J. Nowotarski, J. P. Mulholland, and R. L. Thompson, 2020b: The Influences of Effective Inflow Layer Streamwise Vorticity and Storm-Relative Flow on Supercell Updraft Properties. *J. Atmospheric Sci.*, **77**, 3033–3057, https://doi.org/10.1175/JAS-D-19-0355.1.

Peters, J. M., J. P. Mulholland, and D. R. Chavas, 2021: Generalized lapse rate formulas for use in entraining CAPE calculations. *J. Atmospheric Sci.*, **1**, https://doi.org/10.1175/JAS-D-21-0118.1.

Rasmussen, E. N., and D. O. Blanchard, 1998: A Baseline Climatology of Sounding-Derived Supercell andTornado Forecast Parameters. *Weather Forecast.*, **13**, 1148–1164, https://doi.org/10.1175/1520-0434(1998)013<1148:ABCOSD>2.0.CO;2.

Schultz, L. A., and D. J. Cecil, 2009: Tropical Cyclone Tornadoes, 1950–2007. *Mon. Weather Rev.*, **137**, 3471–3484, https://doi.org/10.1175/2009MWR2896.1.

Sueki, K., and H. Niino, 2016: Toward better assessment of tornado potential in typhoons: Significance of considering entrainment effects for CAPE. *Geophys. Res. Lett.*, **43**, 12,597-12,604, https://doi.org/10.1002/2016GL070349.

Thompson, R. L., R. Edwards, J. A. Hart, K. L. Elmore, and P. Markowski, 2003: Close Proximity Soundings within Supercell Environments Obtained from the Rapid Update Cycle. *Weather Forecast.*, **18**, 1243–1261, https://doi.org/10.1175/1520-0434(2003)018<1243:CPSWSE>2.0.CO;2.

THIS PAGE INTENTIONALLY LEFT BLANK

INITIAL DISTRIBUTION LIST

1. Defense Technical Information Center
   Ft. Belvoir, Virginia

2. Dudley Knox Library
   Naval Postgraduate School
   Monterey, California